CNO enrichment by rotating AGB stars in globular clusters

T. Decressin[1,2], C. Charbonnel[1,3], L. Siess[4,5], A. Palacios[6], G. Meynet[1], and C. Georgy[1]

1 Geneva Observatory, University of Geneva, 51, ch. des Maillettes, CH-1290 Versoix, Switzerland
2 Argenlader Institut für Astronomie (AIfA), Universität Bonn, Auf dem Hügel 71, D-53121 Bonn, Germany
3 Laboratoire d'Astrophysique de Toulouse-Tarbes, CNRS UMR 5572, Université de Toulouse, 14, Av. E.Belin, F-31400 Toulouse, France
4 Institut d'Astronomie et d'Astrophysique, Université Libre de Bruxelles, ULB - CP 226, B-1050 Brussels, Belgium
5 Centre for Stellar and Planetary Astrophysics, School of Mathematical Sciences, Monash University, Victoria 3800, Australia
6 Groupe de Recherche en Astronomie et Astrophysique du Languedoc, UMR 5024, Université Montpellier II, CNRS, place Eugène Bataillon, 34095 Montpellier, France

ABSTRACT

Context. AGB stars have long been held responsible for the important star-to-star variations in light elements observed in Galactic globular clusters.

Aims. We analyse the main impacts of a first generation of rotating intermediate-mass stars on the chemical properties of second-generation globular cluster stars. The rotating models were computed without magnetic fields and without the effects of internal gravity waves. They account for the transports by meridional currents and turbulence.

Methods. We computed the evolution of both standard and rotating stellar models with initial masses between 2.5 and 8 $M_\odot$ within the metallicity range covered by Galactic globular clusters.

Results. During central He-burning, rotational mixing transports fresh CO-rich material from the core towards the hydrogen-burning shell, leading to the production of primary ^{14}N. In stars more massive than $M \gtrsim 4 M_\odot$, the convective envelope reaches this reservoir during the second dredge-up episode, resulting in a large increase in the total C+N+O content at the stellar surface and in the stellar wind. The corresponding pollution depends on the initial metallicity. At low- and intermediate-metallicity (i.e., [Fe/H] lower than or equal to ~ -1.2), it is at odds with the constancy of C+N+O observed among globular cluster low-mass stars.

Conclusions. With the given input physics, our models suggest that massive (i.e., ≥ 4 $M_\odot$) rotating AGB stars have not shaped the abundance patterns observed in low- and intermediate-metallicity globular clusters. Our non-rotating models, on the other hands, do not predict surface C+N+O enhancements, hence are in a better position as sources of the chemical anomalies in globular clusters showing the constancy of the C+N+O. However at the moment, there is no reason to think that intermediate mass stars were not rotating. On the contrary there is observational evidence that stars in clusters have higher rotational velocities than in the field.

Key words. stars: AGB and post-AGB, rotation, abundances - globular clusters: general

1. Introduction

While the abundances of heavy elements (i.e., Fe-group and α-elements) are fairly constant from star-to-star in any well-studied individual Galactic globular cluster (GC)[1], giant and turnoff stars present some striking anomalies in their light elements content (Li, F, C, N, O, Na, Mg, and Al) that are not shared by their field counterparts (for a review see Gratton 2007). Important is that the sum [(C+N+O)/Fe] for individual GC stars otherwise presenting very different chemical features is constant to within experimental errors in all the clusters studied so far, with the possible exception of NGC 1851 (for references see §5).

We now have compelling evidence that these peculiar chemical patterns were present in the intracluster gas from which second-generation (anomalous) low-mass stars formed, and that they resulted from the dilution of pristine material with the hydrogen-burning products ejected by a first generation of more massive and faster evolving GC stars (for a review see Prantzos et al. 2007).

Massive AGB stars that undergo efficient hot-bottom burning (HBB) during the thermal pulse phase (TP-AGB) have been proposed as the possible GC polluters in this so-called self-enrichment scenario (Ventura et al. 2001). The AGB hypothesis has been extensively discussed in the literature, first on a qualitative basis, and more recently with the help of custom-made standard (i.e., non-rotating) stellar models (Ventura et al. 2001, 2002; Ventura & D'Antona 2005a,b,c, 2008a,b; Denissenkov & Herwig 2003; Karakas & Lattanzio 2003; Herwig 2004a,b; Fenner et al. 2004; Bekki et al. 2007). These studies point out several difficulties in building the observed chemical patterns in theoretical TP-AGB models. The main problem stems from to the competition between the third dredge-up (3DUP) that contaminates the AGB envelope with the helium-burning ashes produced in the thermal pulse and HBB that modifies the envelope abundances via the CNO-cycle and the NeNa- and MgAl-chains. It is thus very difficult to obtain simultaneous O depletion and Na enrichment in the TP-AGB envelope, while keeping the C+N+O sum constant as required by the observations (see Charbonnel 2007, for more details and references).

To date, only AGB models in the mass range 5-6.5 $M_\odot$ have managed to simultaneously achieve an encouraging agreement with the observed O-depletion and the Na-enrichment (Ventura

---

1 Except ω Cen (Norris & Da Costa 1995; Johnson et al. 2008).

& D'Antona 2008a). These models include the FST formulation for convection (Canuto et al. 1996), which strongly affects the O depletion once the stars enter the TP-AGB (Ventura & D'Antona 2005b). Compared to the classical MLT treatment, FST indeed leads to higher temperatures at the base of the convective envelope (resulting in more advanced nucleosynthesis) and induces higher surface luminosities resulting in stronger mass loss and thus fewer thermal pulses and 3DUP events. As shown by Ventura & D'Antona (2005b), some O depletion can also be obtained with the MLT prescription, but only when the free parameter α is arbitrarily and strongly modified with respect to the value calibrated on the Sun. These models are also able to produce a slight decrease in Mg accompanied with a large increase in Al.

The Na-enrichment is more difficult to estimate and requires fine tuning of the NeNa-cycle reaction rates. More precisely, an increase in sodium is achieved in the most oxygen-poor ejecta of the 5-6.5 $M_\odot$ models only when the maximum allowed values for the ^{22}Ne(p,γ) rate are adopted. In summary, and as clearly stated by Ventura & D'Antona (2008a), the AGB scenario is viable from the nucleosynthesis point of view, provided that only massive AGB stars of 5 to 6.5 $M_\odot$ contribute to the GC self-enrichment, and under the physical assumptions described above.

However the previously quoted models have only focused on physical uncertainties related to the TP-AGB phase, and their predictions have not been tested in different astrophysical contexts. In particular, the impact of rotation in our models on the nucleosynthesis predictions for AGB stars has never been investigated in the context of the GC self-enrichment scenario, although rotation is often invoked to understand a wide variety of observations (e.g. Maeder & Meynet 2000, 2006; Chiappini et al. 2008, see § 4). The present paper addresses this question for the first time, using up-to-date treatment for rotation-induced processes. As we shall see, the main signature of rotation on the chemical composition of the stellar envelope and winds of intermediate-mass stars already show up during the second dredge-up event and cannot be erased during the TP-AGB phase.

2. Physical input of the stellar models

Although only massive AGB stars in a very narrow mass range between 5 and 6.5 $M_\odot$ are now suspected to play a role in the self-enrichment scenario (Ventura & D'Antona 2008a,b), we computed standard and rotating models of 2.5, 3, 4, 5, 7, and 8 $M_\odot$ stars with the code STAREVOL (V2.75) (Siess et al. 2000; Siess 2006). We present results for several metallicities, namely $Z = 4 \times 10^{-3}$, 10^{-3}, 5×10^{-4}, 10^{-4}, and 10^{-5} (i.e., [Fe/H]$\simeq$ -0.66, -1.26, -1.56, -2.26, and -3.26 respectively)[2]. The composition is scaled solar according to the Grevesse & Sauval (1998) mixture and enhancement in α-elements ([α/Fe] = +0.3 dex) is accounted for. All models were evolved up to the completion of the 2DUP.

We used the OPAL opacity tables (Iglesias & Rogers 1996) above $T > 8000$ K that account for C and O enrichments, and the Ferguson et al. (2005) data at lower temperatures. We followed the evolution of 53 chemical species from ^{1}H to ^{37}Cl using the NACRE nuclear reaction rates (Angulo et al. 1999) by

default and those by Caughlan & Fowler (1988) otherwise (see Siess & Arnould 2008). The treatment of convection is based on the classical mixing length formalism with $\alpha_{MLT} = 1.75$, and no convective overshoot is included. The mass loss rates are computed with Reimers (1975) formula (with $\eta_R = 0.5$).

For the treatment of rotation-induced processes we proceed as follows. Solid-body rotation is assumed on the ZAMS and a typical initial surface velocity of 300 km s^{-1} is chosen for all the models. (The impact of this choice is discussed in § 3.3 where we present models computed with initial rotation velocities ranging from 50 to 500 km s^{-1}.) On the main sequence, the evolution of the internal angular momentum profile is accounted for with the complete formalism developed by Zahn (1992) and Maeder & Zahn (1998) (see Palacios et al. 2003, 2006; Decressin et al. 2009 for a description of the implementation in STAREVOL), which takes advection by meridional circulation and diffusion by shear turbulence into account. The initial solid-body profile relaxes on the main sequence on a short timescale of a few Myr and generates differential rotation. For our most massive stellar models ($M \geq 4$ $M_\odot$), the complete formalism for angular momentum transport is applied up to the 2DUP. For the lower mass models, however, the complete treatment is only applied up to the end of the main sequence, while a more crude approach is used in the more advanced evolution phases where angular momentum evolves only through local conservation (i.e. only the structural changes modify the angular momentum). This simplification is motivated by the evolutionary timescale (i.e., the Kelvin-Helmholtz timescale on the RGB) becoming shorter than the meridional circulation timescale. We test this assumption by running a 5 and 7 $M_\odot$ with and without the full treatment of rotational mixing and the results show little difference, validating our approximation. In all cases the transport of chemical species resulting from meridional circulation and both vertical and horizontal turbulence is computed as a diffusive process (Chaboyer & Zahn 1992) throughout the evolution.

3. Signatures of rotation-induced mixing up to the early-AGB phase

3.1. Models at [Fe/H]=-1.56

Up to the beginning of the TP-AGB phase, the surface composition of the standard models is only modified by the dredge-up event(s). Let us note that only the 2.5 and 3 $M_\odot$ models undergo deep enough first dredge-up so as to modify their surface abundances; however, all stars experience to various extents the second dredge-up (hereafter 2DUP) after central He exhaustion. As described below, in the rotating models the effects of additional mixing become visible at the stellar surface during the quiescent central He-burning phase.

Figure 1 shows the abundance profiles (in mass fraction) of ^{1}H, ^{4}He, ^{12}C, ^{14}N, and ^{16}O, as well as the total sum C+N+O, at the end of central He-burning and before the 2DUP, for standard (lower row) and rotating (upper row) 5 $M_\odot$ model.

In the standard case, ^{14}N steadily increases as one moves inwards through the H-rich radiative layers down to the He buffer (located between $M_r \sim 0.7$ and 1.2 $M_\odot$) as a result of CNO processing. Further inside, the stellar core has experienced complete He-burning and is essentially made of ^{16}O and ^{12}C. In this 5 $M_\odot$ model, during the 2DUP, the convective envelope penetrates into the He-rich buffer (down to $M_r \simeq 0.85$ $M_\odot$) as indicated by the hatched area. This produces an envelope enrichment in H-burning ashes: the surface abundances of ^{12}C and ^{16}O decrease, while that of ^{14}N and ^{4}He increase. The sum C+N+O, however,

---

[2] The models at [Fe/H]$\simeq$ -0.66 and -3.26 are actually from Maeder & Meynet (2001) and Meynet & Maeder (2002), respectively. To check the consistency of our predictions with those of the Geneva code, we computed a 7 $M_\odot$ model at $Z = 10^{-5}$ with STAREVOL and found excellent agreement in terms of both evolutionary and chemical characteristics (see Fig. 2).
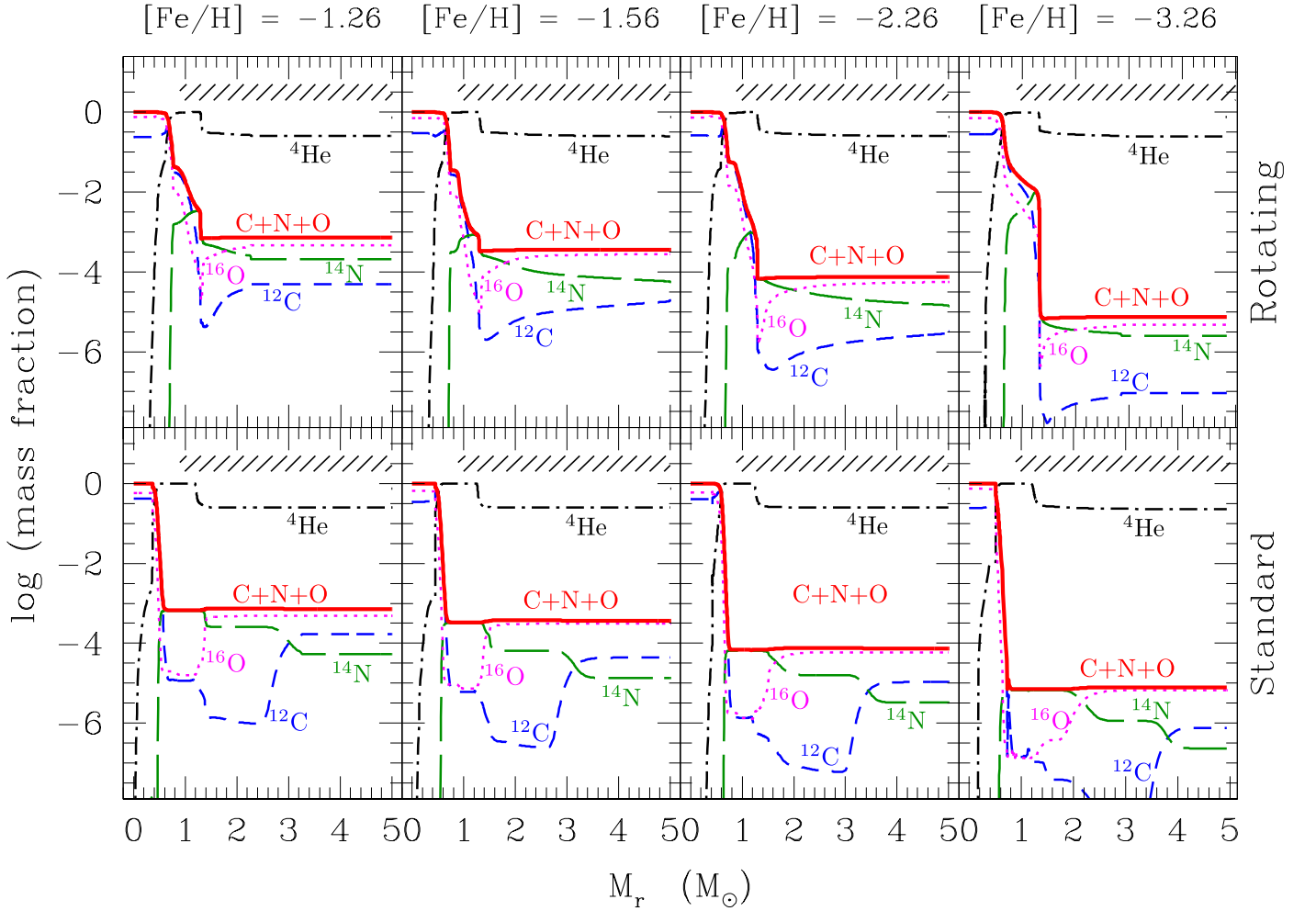
Fig. 1. Chemical profiles (in mass fraction) at the end of central He-burning in rotating (top) and standard (bottom) 5 $M_\odot$ models at $Z = 0.001$, 0.0005, 0.0001, and 0.00001 (left to right). The elements shown are ^{4}He (dotted-dashed lines), ^{12}C (short-dashed lines), ^{14}N (long-dashed lines), ^{16}O (dotted lines), sum C+N+O (thick lines). The hatched area on top of each panel indicates the maximum extent of the convective envelope during the 2DUP.

remains constant, since only the H-burning products are dredged up.

Rotation-induced mixing strongly modifies the internal chemical structure. As shown in the upper-row panels of Fig. 1, the abundance gradients are smoothed out in the radiative envelope (i.e., the region above the He-rich buffer up to the surface or the convective envelope) compared to the standard case: ^{14}N produced in the internal H-burning layers diffuses outwards, while the ^{12}C and ^{16}O present in the envelope are transported inwards. As a consequence, during the whole central He-burning phase, rotational mixing produces a continuous surface increase in ^{14}N concomitant to a decrease in ^{12}C and ^{16}O. At the same time, the products of central helium-burning, namely ^{12}C and ^{16}O, also diffuse outward in the He-rich buffer (i.e., the region where He is the dominant species, between 0.6 and 1.4 $M_\odot$ in Fig. 1).

The transport of chemical species is mainly driven by shear turbulence ($D_{\rm shear} \sim 10^8$ cm s^{-1}) in the radiative envelope and in the He-rich layer. At the interface of these two regions, i.e. at the base of the HBS, the large mean molecular weight gradient strongly reduces the efficiency of mixing ($D_{\rm shear} \sim 10^3$ cm s^{-1}), thus preventing the transport of primary C, N, and O from the He-rich buffer to the HBS, hence thus to the surface during central He-burning. At the same time, hydrogen from the envelope is also transported inwards and rapidly captured by ^{12}C and ^{16}O nu-

clei through CNO burning at high temperature. This leads to the production of a peak of *primary* ^{14}N at the base of the hydrogen-burning shell (HBS) as seen in Fig. 1. The resulting chemical profiles at the end of central He-burning thus differ significantly from those obtained in the standard case where ^{14}N is only produced in the HBS from the ^{12}C and ^{16}O originally present in the star and is therefore of secondary origin (Meynet & Maeder 2002). During the subsequent 2DUP, the convective envelope of the 5 M$_\odot$ rotating model reaches the polluted He-rich buffer (see Fig. 1) producing a large increase in ^{4}He. Simultaneously the primary CNO and thus the overall metallicity increases in the envelope.

In the 2.5 and 3 $M_\odot$ rotating models, the convective envelope does not reach the contaminated He-buffer during the 2DUP. As a consequence in these low-mass models, only the H-burning products are dredged up to the surface: ^{14}N strongly increases, while ^{12}C and ^{16}O decrease, but the sum C+N+O, as well as the total metallicity, remain unchanged (see Table 1). ^{4}He also diffuses outward into the radiative envelope leading to a surface ^{4}He enhancement by about 0.03 (in mass fraction) compared to non-rotating models.

Table 1 summarises the abundance variations after the 2DUP in all our standard and rotating models at [Fe/H]=-1.56. The main signature of rotational mixing at the surface of massive

Table 1. Surface abundance variations after the completion of the 2DUP with respect to the initial composition (δ[X/Fe] = [X/Fe]$_{2DUP}$ − [X/Fe]$_{init}$) for the models with initial value of [Fe/H]=-1.56

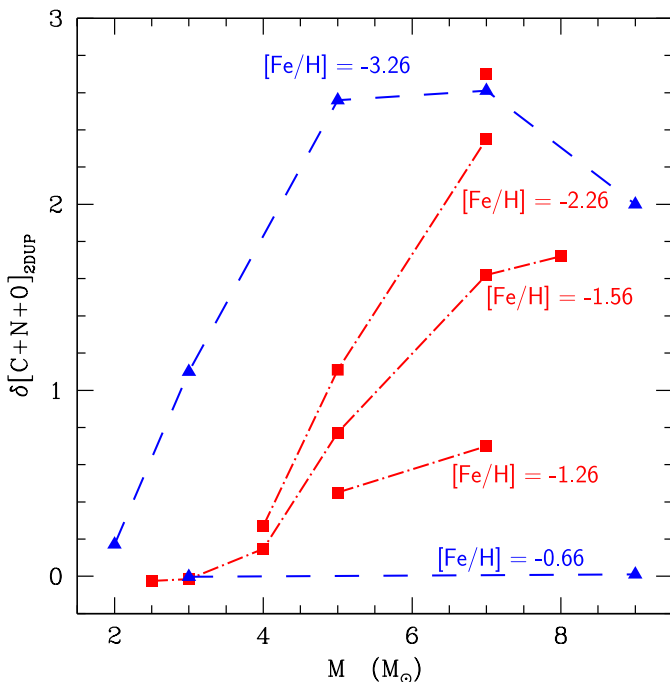|	2.5 $M_\odot$	3 $M_\odot$	4 $M_\odot$	5 $M_\odot$	7 $M_\odot$	8 $M_\odot$
			Standard models			
He	0.26	0.26	0.29	0.32	0.36	0.36
δ[C/Fe]	-0.20	-0.25	-0.29	-0.31	-0.30	-0.34
δ[N/Fe]	0.44	0.48	0.60	0.75	0.79	0.81
δ[O/Fe]	-0.01	-0.01	-0.03	-0.06	-0.10	-0.11
δ[CNO/Fe]	0.00	0.00	0.00	0.00	0.00	0.00
			Rotating models			
He	0.29	0.29	0.32	0.34	0.35	0.36
δ[C/Fe]	-1.12	-0.86	-0.20	1.44	2.14	2.16
δ[N/Fe]	1.23	1.12	1.13	1.24	1.19	1.09
δ[O/Fe]	-0.65	-0.36	-0.01	0.18	1.46	1.55
δ[CNO/Fe]	0.00	0.00	0.15	0.78	1.62	1.71

Fig. 2. Surface C+N+O increase index (δ[C+N+O]$_{2DUP}$ = [C+N+O/Fe]$_{2DUP}$ − [C+N+O/Fe]$_{init}$) at the end of the 2DUP for rotating stars with various initial masses and metallicities. Squares and triangles indicate models computed with STAREVOL and with the Geneva code, respectively (see text for details).
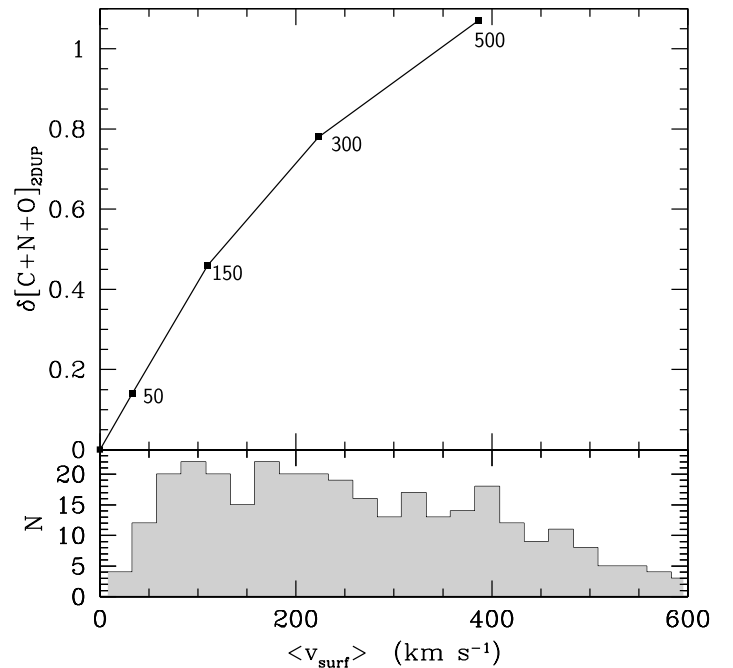

Fig. 3. *Top:* enrichment in C+N+O after the 2DUP completion as a function of the mean main sequence velocity for a 5 $M_\odot$, $Z = 0.0005$ for initial surface velocities of 0, 50, 150, 300, 500 km s^{-1} as indicated. *Bottom:* distribution of surface velocities observed by Martayan et al. (2006) in the young LMC cluster NGC 2004 for B-type stars with mass from 2 to 10 $M_\odot$ ($v \sin i$ measurements are multiplied by a factor $4/\pi$).

early-AGB stars ($M \geq 4\ M_\odot$) is a strong increase in He-burning products, i.e., primary CNO (see also Fig. 2). As all rotating models produce an enrichment of CNO elements inside the He-buffer, the total increase of C+N+O at the surface of rotating models mainly depends on the depth reached by the convective envelope during the 2DUP. We thus obtain a stronger variation with increasing stellar mass.

3.2. Influence of metallicity

The impact of rotation on stellar properties and stellar yields is known to depend strongly on metallicity (see, e.g., Meynet & Maeder 2002). The metallicity dependence of our predictions is depicted in Fig. 1 showing the internal profiles of ^{12}C, ^{14}N, and ^{16}O at the end of central He-burning in standard and rotating 5 $M_\odot$ models at four different metallicities ([Fe/H] $\simeq$ −1.26,

−1.56, −2.26, and −3.26). As previously explained, the C+N+O profile outside the CO core is constant in the standard models, while it strongly increases in the He-rich layers below the HBS in the rotating models. This C+N+O step is higher in lower metallicity stars, which results in a stronger CNO surface enrichment after 2DUP in the most metal-poor stars as shown in Fig. 2. The maximal depth reached by the convective envelope for a given stellar mass hardly depend on metallicity; e.g., it reaches 1.04 and 1.07 $M_\odot$ for the 7 $M_\odot$ at $Z = 10^{-3}$ and $Z = 10^{-4}$.

At [Fe/H]=-2.26, the envelope (and thus the wind) of all the stars more massive than $\sim 5 M_\odot$ undergo a C+N+O increase by 1 to 2 orders of magnitude, while an increase by a factor of 5 is obtained at [Fe/H] = −1.26. When metallicity becomes higher than [Fe/H] $\simeq$ −1, rotation-induced mixing increases the total C+N+O by less than a factor 2-3, which is undetectable with current observations (see § 5). The effect is null at [Fe/H] = −0.66.

3.3. Influence of initial rotation velocity

We present several models for the 5 $M_\odot$ star at $Z = 0.0005$ ([Fe/H] = −1.56) with initial rotation velocities between 0 and 500 km s^{-1} as part of investigating the dependence of our results on this parameter. As shown in Fig. 3, the C+N+O enhancement increases with increasing initial rotation. A higher initial velocity leads to a faster spinning core and to a larger differential rotation at the core edge during central He-burning. Since mixing stems mainly from shear turbulence and scales as $(\partial\Omega/\partial r)^2$ (Talon & Zahn 1997), more CNO elements are stored in the He-rich buffer and then revealed at the surface after 2DUP. In the model with an initial velocity of 150 km s^{-1}, the C+N+O rises by a factor 3, while it increases by more than a factor 14 for an initial velocity of 500 km s^{-1}.

4. Discussion on the model uncertainties

4.1. Mean rotation velocity

As shown above, the total C+N+O enhancement depends on the assumed initial rotational velocity. We note that, for an initial (i.e., ZAMS) velocity of 300 km s^{-1}, the time-averaged velocity of our models on the main sequence ranges between 220 and 256 km s^{-1} depending on the stellar mass and metallicity. What are the observational constraints on this ingredient?

Martayan et al. (2006, 2007a) find mean $v \sin i$ of 161 $\pm$ 20 km s^{-1} and 155 $\pm$ 20 km s^{-1} for SMC B-type stars of 2–5 $M_\odot$ (111 stars) and 5–10 $M_\odot$ (81 stars), respectively. Accounting in a statistical way for the $\sin i$ effect (i.e. multiplying the averaged $v \sin i$ by $4/\pi$ supposing a random distribution of the rotational axis), we obtain averaged values for v between 197 and 205 km s^{-1} for B-type stars in the SMC. At first glance, the main-sequence time-averaged velocity of our models is slightly higher than the observed values for SMC stars. However, the following points have to be considered:

1. The mean observed values quoted above do not account for Be-type stars. Let us recall that Be stars are fast rotators that present emission lines originating in an outward equatorial expanding disk probably formed due to strong stellar rotation (Martayan et al. 2007b). Therefore Be stars belong to the upper part of the velocity distribution, and it is legitimate to incorporate them in the estimate of the averaged velocities of B-type stars. Taking them into account does enhance the observed average velocities. As an illustrative example, the mean $v \sin i$ for SMC Be stars in the mass ranges 2–5, 5–10 $M_\odot$ are 277 $\pm$ 34 km s^{-1} (14 stars) and 297 $\pm$ 25 km s^{-1} (81 stars), respectively. As can be seen in Fig. 3, our assumptions on the stellar rotation velocities are thus totally realistic;

2. Martayan et al. (2007a) (see also Hunter et al. 2008b) find that, for both B and Be stars, the lower the metallicity, the higher the rotational velocities. This agrees with the finding by Maeder et al. (1999) and Wisniewski & Bjorkman (2006) that the fraction of Be stars with respect to the total number of B+Be stars increases when the metallicity decreases. Since the metallicities considered in this work are lower than that of the SMC, we may expect that the averaged velocities of the stars would be somewhat higher than the one quoted above for the SMC;

3. Last but not least, there is evidence that the rotation rates of stars are higher in clusters than in the field (Keller 2004; Huang & Gies 2005; Strom et al. 2005; Dufton et al. 2006; Wolff et al. 2007).

Thus, in view of these remarks, it does appear that our adopted rotation velocities are probably very close to the averaged velocities of stars in clusters for the range of masses and metallicities considered. If the previous extrapolations are correct, the values given in Fig. 2 should be considered as lower limits.

4.2. Treatment of rotation

Of course, rotating models are not free from uncertainties and their predictions should be carefully compared with well-observed features. The physics included in the present models is the same as the one that provides a good fit to the following observed features:

– the surface enrichments in nitrogen in main-sequence B-type stars (Maeder et al. 2009), even if invoking binarity or mag-

netic fields is required to explain the whole observational pattern (Hunter et al. 2008a);
– the observed number ratio of blue to red supergiants in the SMC (Maeder & Meynet 2001);
– the variation with the metallicity of the number fraction of WR to O-type stars (Meynet & Maeder 2003, 2005);
– the variation with metallicity of the number ratio of type Ibc to type II core collapse supernovae (Meynet & Maeder 2005).
– the lithium abundance patterns in A-type and early F-type dwarf stars, as well as in their subgiant descendants (Charbonnel & Talon 1999; Palacios et al. 2003).

Moreover, they provide a reasonable explanation for the origin of the high N/O observed at the surface of metal-poor halo stars, as well as for the C/O upturn (Chiappini et al. 2006, 2008). Therefore, while the present models are not free of uncertainties, they have the nice property of accounting for the above observed features.

4.3. Rotational rate of remnants

The present models have some difficulty, however, in accounting for the observed rotation rates of young pulsars and white dwarfs (see e.g. Kawaler 1988; Heger et al. 2005; Suijs et al. 2008). More precisely, they predict too fast rotation of the stellar cores in the advanced phases. This may be stem from different causes that could lead to additional angular momentum loss from the central regions at different evolutionary phases:

– already during the nuclear lifetime;
– at the time of the supernova explosion in the case of neutron stars or during the TP-AGB phase at the time of the super-wind episode in the case of white dwarfs;
– by the neutron stars or the white dwarfs themselves shortly after their formation.

In the second and third cases mentioned above, the physics and the predictions of the present models would not need to be revised since the loss of angular momentum would occur after the evolutionary stages covered by the present computations. However, if the loss of angular momentum occurs before second dredge-up, another mechanism should be included at earlier phases in rotating models.

The study of the s-process nucleosynthesis in low-mass TP-AGB stars could provide some hints to the rotational evolution of the stellar core. At the moment the properties and the behaviour of rotating TP-AGB stars are poorly known. Calculations using a diffusive treatment for the transport of angular momentum by Langer et al. (1999), Herwig et al. (2003), and Siess et al. (2004) have shown that rotationally induced instabilities provide enough mixing to trigger the 3DUPs. However, a shear layer at the base of the convective envelope leads to an efficient pollution of the ^{13}C pocket[3] (the neutron source) by ^{14}N with the result of strongly inhibiting the s-process nucleosynthesis. This is at odds with the observations of s-stars and tends to indicate that the modeling of rotation used in these models needs to be improved and that angular momentum must have been removed by the time the thermal pulses start. Therefore, if the extraction of angular momentum occurs before core helium burning, no CNO enrichment will be expected because it relies on shear due to a fast spinning core. On the other hand, if the extraction occurs

---

[3] In this framework, the neutrons needed for the s-process are released in the ^{13}C pocket by ^{13}C(α,n) reaction.

during the early-AGB phase, it could allow both the CNO enrichment of the He-buffer and the s-process during the TP-AGB phase.

The mechanism frequently pointed to for removing angular momentum from the core is the magnetic field. For instance, Heger et al. (2005) have shown that magnetic coupling between the core and envelope can account for the rotation rates of young neutron stars. Suijs et al. (2008) also find that magnetic torques may be required to understand the slow spin rate of white dwarfs. However the dynamo model (Spruit 2002) on which the current rotating models with magnetic fields are based has recently been tested through hydrodynamical computations by Zahn et al. (2007), who do not find the amplification of the magnetic field as expected from the theory, casting some doubt on its validity. In view of the remaining theoretical uncertainties associated with the treatment of magnetic fields, it seems reasonable to stick to the present models whose predictions account for a broad variety of observations as described in § 4.2.

Finally let us note that Talon & Charbonnel (2008) predict that angular momentum transport by internal gravity waves should be efficient in intermediate-mass stars during the early-AGB phase. If these waves were the culprit, then the predictions of the present models would be valid as far as the CNO enrichment is concerned since it builds up earlier in the life of the star.

5. Consequences for the self-enrichment scenario

5.1. Summary of the theoretical predictions

During central He-burning, rotational mixing efficiently transports primary ^{12}C and ^{16}O outside the convective core in the H-burning region where these elements are processed by the CNO cycle, resulting in an important production of primary ^{14}N. In the massive ($M \gtrsim 4M_\odot$) rotating models, after central He-exhaustion, the convective envelope penetrates into the layers affected by rotation-induced mixing. In contrast to standard models, the 2DUP produces a large surface enrichment in total C+N+O that cannot be erased by hot bottom (hydrogen) burning during the subsequent TP-AGB evolution. Third dredge-up episodes further increase the total C+N+O mass fraction as they bring the products of He-burning to the surface.

As a consequence, if rotating massive AGB stars were responsible for the abundance patterns observed in GCs, one would expect large C+N+O differences between (O-rich and Na-poor) first-generation stars and (O-poor and Na-rich) second-generation stars (see e.g. Prantzos & Charbonnel 2006). Such differences would easily amount to 1.6 dex in GCs with [Fe/H]∼-1.5, and to 2.2 dex in the most metal-poor clusters with [Fe/H]∼-2.2 for the cases where the ejecta of the first-generation would not have been diluted with pristine material. Diluting these ejecta with 10 times more pristine material would still give differences of 0.6 to 1.2 dex, well above the observed dispersion (see § 5.2). Actually, to maintain C+N+O constant would require such a high dilution of the ejecta with the intracluster matter that the O-Na and Mg-Al anticorrelations would be erased and, as far as abundances are concerned, first and second generation stars would be indistinguishable.

5.2. Comparison with the observations

C, N, and O abundances have been determined simultaneously in stars of several GCs. Up to now, no significant star-to-star variation of the total C+N+O has been detected, except in NGC 1851.

In the case of the most metal-rich GCs such as 47 Tuc (Carretta et al. 2005) and NGC 6712 (Yong et al. 2008), this C+N+O constancy is actually compatible with pollution by both standard and rotating AGB stars since the 2DUP CNO enrichment is found to be negligible in the most metal-rich rotating models. This is of course without considering possible C+N+O increase due to the 3DUP of He-processed material during the TP-AGB phase, which is beyond the scope of the present study.

In the case of intermediate-metallicity ([Fe/H] ∼ −1.2) GCs, such as NGC 288 and NGC 362 (Dickens et al. 1991) and M4 (Ivans et al. 1999; Smith et al. 2005), the total C+N+O is found constant from star to star, within observational uncertainties that amount to ±0.25–0.3 dex. At this metallicity, the most massive intermediate-mass rotating models ($M \gtrsim 5$) predict a C+N+O increase between 0.5 and 0.7 dex at odds with the observations. The only exception is NGC 1851 (Yong et al. 2009, [Fe/H] ∼ −1.2), where variations in the total CNO by 0.57 ± 0.15 dex were found, which is compatible with the CNO enrichment produced by our rotating models as shown in Fig. 2. We note, however, that the stars observed by Yong and collaborators in NGC 1851 are very bright objects. In view of its position in the colour-magnitude diagram, the only star with C+N+O exceeding the typical error bar could actually be an AGB star. In that case, the high value of the total CNO may not have been inherited at birth by the star, but may instead be due to nuclear processes within the star itself. Being an AGB would also explain why this star is the only one among the sample to exhibit some enhancement in s-process elements. We note that in this cluster a double subgiant branch has been detected by photometric measurements (Milone et al. 2008) that can be interpreted as caused by an age difference among cluster stars of about 1 Gyr [4]. However, Cassisi et al. (2008) propose to fit the double sequence assuming two coeval cluster stellar populations with a C+N+O difference of a factor of 2. CNO measurements in NGC 1851 unevolved stars (as done in most of the other clusters studied so far) are thus crucial for settling the problem.

Finally, the CNO predictions for the rotating most massive intermediate mass models lead to increasing factors up to 10 (5 $M_\odot$) and 100 (7 $M_\odot$) at low-metallicity ([Fe/H] = −2.2), in clear contradiction with the observations in the metal-poor clusters studied so far, i.e., M3 and M13 (Smith et al. 1996; Cohen & Meléndez 2005), NGC 6752, and NGC 6397(Carretta et al. 2005)[5]. CNO measurements in other very metal-poor globular clusters like M15 or M92 would be extremely valuable in this context.

6. Conclusions

In this paper we have investigated the effects of rotation in low-metallicity intermediate-mass stars during their evolution up to the completion of the 2DUP and arrival on the AGB. Our rotating stellar models include the complete formalism developed by Zahn (1992) and Maeder & Zahn (1998) and accounts for the transport of chemicals and angular momentum by meridional circulation and shear turbulence. With respect to standard models, the most important change concerning the nucleosynthesis is

---

[4] The hypothesis of two populations with similar age and [Fe/H] differing beyond the errorbars have been ruled out by the spectroscopic study of RGB stars by Yong et al. (2009) and by the photometric study of RR Lyrae by Walker (1998).

[5] NGC 6397 ([Fe/H] ∼ −1.95) does not show a very extended O-Na anticorrelation, a more modest C+N+O increase is expected in that case.

the large ^{14}N production resulting from the diffusion of protons below the HBS in a region enriched with primary C and O during central He-burning. During the subsequent 2DUP, the convective envelope of massive AGB stars deepens in this region, producing a large surface increase in the total C+N+O, which irreversibly imprints the yields.

This behaviour is in sharp contrast to what is observed in low- and intermediate-metallicity globular clusters where the sum C+N+O is constant within the experimental errors. Our rotating models based on the Zahn (1992) formalism, which neglect the effects of magnetic fields and internal gravity waves, thus suggesting that massive rotating AGB stars can be discarded as potential polluters in the self-enrichment scenario in globular clusters, unless the crowded environment prevented intermediate-mass stars from rotating. This latest hypothesis is highly improbable in view of the observations finding higher stellar rotation velocities in clusters than in the field.

References

Angulo, C., Arnould, M., Rayet, M., et al. 1999, Nuclear Physics A, 656, 3
Bekki, K., Campbell, S. W., Lattanzio, J. C., & Norris, J. E. 2007, MNRAS, 267
Canuto, V. M., Goldman, I., & Mazzitelli, I. 1996, ApJ, 473, 550
Carretta, E., Gratton, R. G., Lucatello, S., Bragaglia, A., & Bonifacio, P. 2005, A&A, 433, 597
Cassisi, S., Salaris, M., Pietrinferni, A., et al. 2008, ApJ, 672, L115
Caughlan, G. R. & Fowler, W. A. 1988, Atomic Data and Nuclear Data Tables, 40, 283
Chaboyer, B. & Zahn, J.-P. 1992, A&A, 253, 173
Charbonnel, C. 2007, in Astronomical Society of the Pacific Conference Series, Vol. 378, Why Galaxies Care About AGB Stars: Their Importance as Actors and Probes, ed. F. Kerschbaum, C. Charbonnel, & R. F. Wing, 416–+
Charbonnel, C. & Talon, S. 1999, A&A, 351, 635
Chiappini, C., Ekström, S., Meynet, G., et al. 2008, A&A, 479, L9
Chiappini, C., Hirschi, R., Meynet, G., et al. 2006, A&A, 449, L27
Cohen, J. G. & Meléndez, J. 2005, AJ, 129, 303
Decressin, T., Mathis, S., Palacios, A., et al. 2009, A&A, 495, 271
Denissenkov, P. A. & Herwig, F. 2003, ApJ, 590, L99
Dickens, R. J., Croke, B. F. W., Cannon, R. D., & Bell, R. A. 1991, Nature, 351, 212
Dufton, P. L., Ryans, R. S. I., Simón-Díaz, S., Trundle, C., & Lennon, D. J. 2006, A&A, 451, 603
Fenner, Y., Campbell, S., Karakas, A. I., Lattanzio, J. C., & Gibson, B. K. 2004, MNRAS, 353, 789
Ferguson, J. W., Alexander, D. R., Allard, F., et al. 2005, ApJ, 623, 585
Gratton, R. G. 2007, in Astronomical Society of the Pacific Conference Series, Vol. 374, From Stars to Galaxies: Building the Pieces to Build Up the Universe, ed. A. Vallenari, R. Tantalo, L. Portinari, & A. Moretti, 147–+
Grevesse, N. & Sauval, A. J. 1998, Space Science Reviews, 85, 161
Heger, A., Woosley, S. E., & Spruit, H. C. 2005, ApJ, 626, 350
Herwig, F. 2004a, ApJ, 605, 425
Herwig, F. 2004b, ApJS, 155, 651
Herwig, F., Langer, N., & Lugaro, M. 2003, ApJ, 593, 1056
Huang, W. & Gies, D. R. 2005, in Bulletin of the American Astronomical Society, 1273–+
Hunter, I., Brott, I., Lennon, D. J., et al. 2008a, ApJ, 676, L29
Hunter, I., Lennon, D. J., Dufton, P. L., et al. 2008b, A&A, 479, 541
Iglesias, C. A. & Rogers, F. J. 1996, ApJ, 464, 943
Ivans, I. I., Sneden, C., Kraft, R. P., et al. 1999, AJ, 118, 1273
Johnson, C. I., Pilachowski, C. A., Simmerer, J., & Schwenk, D. 2008, ApJ, 681, 1505
Karakas, A. I. & Lattanzio, J. C. 2003, Publications of the Astronomical Society of Australia, 20, 279
Kawaler, S. D. 1988, ApJ, 333, 236
Keller, S. C. 2004, Publications of the Astronomical Society of Australia, 21, 310

Langer, N., Heger, A., Wellstein, S., & Herwig, F. 1999, A&A, 346, L37
Maeder, A., Grebel, E. K., & Mermilliod, J.-C. 1999, A&A, 346, 459
Maeder, A. & Meynet, G. 2000, ARA&A, 38, 143
Maeder, A. & Meynet, G. 2001, A&A, 373, 555
Maeder, A. & Meynet, G. 2006, A&A, 448, L37
Maeder, A., Meynet, G., Georgy, C., & Ekström, S. 2009, in IAU Symposium, Vol. 259, IAU Symposium, 311–322
Maeder, A. & Zahn, J.-P. 1998, A&A, 334, 1000
Martayan, C., Floquet, M., Hubert, A. M., et al. 2007a, A&A, 472, 577
Martayan, C., Frémat, Y., Hubert, A.-M., et al. 2006, A&A, 452, 273
Martayan, C., Frémat, Y., Hubert, A.-M., et al. 2007b, A&A, 462, 683
Meynet, G. & Maeder, A. 2002, A&A, 390, 561
Meynet, G. & Maeder, A. 2003, A&A, 404, 975
Meynet, G. & Maeder, A. 2005, A&A, 429, 581
Milone, A. P., Bedin, L. R., Piotto, G., et al. 2008, ApJ, 673, 241
Norris, J. E. & Da Costa, G. S. 1995, ApJ, 447, 680
Palacios, A., Charbonnel, C., Talon, S., & Siess, L. 2006, A&A, 453, 261
Palacios, A., Talon, S., Charbonnel, C., & Forestini, M. 2003, A&A, 399, 603
Prantzos, N. & Charbonnel, C. 2006, A&A, 458, 135
Prantzos, N., Charbonnel, C., & Iliadis, C. 2007, A&A, 470, 179
Reimers, D. 1975, Circumstellar envelopes and mass loss of red giant stars (Problems in stellar atmospheres and envelopes.), 229–256
Siess, L. 2006, A&A, 448, 717
Siess, L. & Arnould, M. 2008, A&A, 489, 395
Siess, L., Dufour, E., & Forestini, M. 2000, A&A, 358, 593
Siess, L., Goriely, S., & Langer, N. 2004, A&A, 415, 1089
Smith, G. H., Shetrone, M. D., Bell, R. A., Churchill, C. W., & Briley, M. M. 1996, AJ, 112, 1511
Smith, V. V., Cunha, K., Ivans, I. I., et al. 2005, ApJ, 633, 392
Spruit, H. C. 2002, A&A, 381, 923
Strom, S. E., Wolff, S. C., & Dror, D. H. A. 2005, AJ, 129, 809
Suijs, M. P. L., Langer, N., Poelarends, A.-J., et al. 2008, A&A, 481, L87
Talon, S. & Charbonnel, C. 2008, A&A, 482, 597
Talon, S. & Zahn, J.-P. 1997, A&A, 317, 749
Ventura, P. & D'Antona, F. 2005a, A&A, 431, 279
Ventura, P. & D'Antona, F. 2005b, A&A, 431, 279
Ventura, P. & D'Antona, F. 2005c, A&A, 439, 1075
Ventura, P. & D'Antona, F. 2008a, A&A, 479, 805
Ventura, P. & D'Antona, F. 2008b, MNRAS, 385, 2034
Ventura, P., D'Antona, F., & Mazzitelli, I. 2002, A&A, 393, 215
Ventura, P., D'Antona, F., Mazzitelli, I., & Gratton, R. 2001, ApJ, 550, L65
Walker, A. R. 1998, AJ, 116, 220
Wisniewski, J. P. & Bjorkman, K. S. 2006, ApJ, 652, 458
Wolff, S. C., Strom, S. E., Dror, D., & Venn, K. 2007, AJ, 133, 1092
Yong, D., Grundahl, F., D'Antona, F., et al. 2009, ApJ, 695, L62
Yong, D., Meléndez, J., Cunha, K., et al. 2008, ApJ, 689, 1020
Zahn, J.-P. 1992, A&A, 265, 115
Zahn, J.-P., Brun, A. S., & Mathis, S. 2007, A&A, 474, 145